
Article:
Hunter, S.J. orcid.org/0000-0002-9280-1969, Cornel, E.J., Mykhaylyk, O.O. orcid.org/0000-0003-4110-8328 et al. (1 more author) (2020) Effect of salt on the formation and stability of water-in-oil Pickering nanoemulsions stabilized by diblock copolymer nanoparticles. Langmuir, 36 (51). pp. 15523-15535. ISSN 0743-7463

https://doi.org/10.1021/acs.langmuir.0c02742

Effect of salt on the formation and stability of water-in-oil Pickering nanoemulsions stabilized by diblock copolymer nanoparticles

Saul J. Hunter, Erik J. Cornel, Oleksandr O. Mykhaylyk and Steven P. Armes*

[†]Department of Chemistry, Dainton Building, University of Sheffield,
Brook Hill, Sheffield, South Yorkshire, S3 7HF, UK.

ABSTRACT. Sterically-stabilized diblock copolymer nanoparticles are prepared in *n*-dodecane using polymerization-induced self-assembly. Precursor Pickering macroemulsions are then prepared by the addition of water followed by high-shear homogenization. In the absence of any salt dissolved in the aqueous phase, high-pressure microfluidization of such precursor emulsions leads to the formation of relatively large water droplets with DLS measurements indicating a mean diameter of more than 600 nm. However, systemically increasing the aqueous salt concentration produces significantly finer droplets after microfluidization, until a limiting diameter of around 250 nm is obtained at 0.11 M NaCl. The mean size of these aqueous droplets can also be tuned by systematically varying the nanoparticle concentration, applied pressure, and the number of passes through the microfluidizer. The mean number of nanoparticles adsorbed onto each aqueous droplet and their packing efficiency is calculated. SAXS studies conducted on a Pickering nanoemulsion confirms that the aqueous droplets are coated with a loosely-packed monolayer of nanoparticles. The effect of varying the amount of NaCl dissolved in the aqueous droplets on their initial rate of Ostwald ripening is investigated using DLS. Finally, the long-term stability of these water-in-oil Pickering nanoemulsions is examined using analytical centrifugation. The rate of droplet ripening can be substantially reduced by using 0.11 M NaCl instead of pure water. However, increasing the salt concentration up to 0.43 M provides no further improvement in the long-term stability of such nanoemulsions.

* Author to whom correspondence should be addressed (s.p.armes@sheffield.ac.uk)

INTRODUCTION

Emulsions stabilized by particles, or so-called Pickering emulsions, were first recognized in the early 1900s.[1-2] Such particulate emulsifiers confer significantly different properties compared to surfactants.[3] For example, if they are sufficiently large and possess appropriate wettability, solid particles remain irreversibly adsorbed at the oil-water interface, whereas surfactant exchange between the interface and bulk solution occurs within short timescales.[3-5] Moreover, whether an emulsion is of the oil-in-water (o/w) or water-in-oil (w/o) type is dictated by the hydrophilic-hydrophobic balance of a surfactant.[6-7] In contrast, the key parameter for Pickering emulsions is the particle wettability, which is determined by the three-phase contact angle at the interface, θ_w.[3, 8] More hydrophilic particles ($\theta_w < 90°$) typically stabilize oil-in-water (o/w) emulsions, whereas water-in-oil (w/o) emulsions are usually stabilized by more hydrophobic particles ($\theta_w > 90°$).[8-12]

Nanoemulsions comprise very fine droplets with a mean diameter of no more than 200 nm.[13-27] They are much less prone to gravitational creaming or sedimentation than conventional emulsions.[13-14] Moreover, they provide more active formulations when used for drug delivery,[28-31] food technology,[32-33] or cosmetics[34] owing to their significantly higher surface area per unit mass.[13, 15] However, both o/w and w/o nanoemulsions tend to suffer from Ostwald ripening.[19, 35-37] In principle, this instability problem can be suppressed by adding a suitable species to the droplet phase that is highly insoluble in the continuous phase.[38-40] For example, addition of a long hydrocarbon (or wax) to oil droplets enhances the stability of o/w nanoemulsions towards Ostwald ripening.[41-43] In the case of w/o emulsions, the addition of salt to the aqueous phase is known to inhibit mass transfer between water droplets.[44-46]

In recent years, there has been growing interest in o/w Pickering nanoemulsions.[35, 47-54] However, there have been rather fewer reports of the analogous w/o Pickering

nanoemulsions.[55-57] In one notable example, Bollhorst et al.[57] prepared submicrometer-sized colloidosomes *via* self-assembly of metal oxide nanoparticles around water droplets in *n*-decane. Sihler and co-workers[57] utilized ultrasonification to prepare relatively fine w/o emulsions of less than 500 nm diameter using anionic silica nanoparticles, which were rendered sufficiently hydrophobic by adsorption of either cation or non-ionic surfactants.[56] Moreover, nanoparticle adsorption at the oil-water interface was relatively inefficient, with many nanoparticles remaining within the interior of the aqueous droplets.

The development of polymerization-induced self-assembly (PISA) has enabled the convenient synthesis of well-defined diblock copolymer nanoparticles.[58-62] This powerful and versatile technique enables the efficient synthesis of 20-30 nm sterically-stabilized spheres in the form of a concentrated dispersion using reversible addition-fragmentation chain transfer (RAFT) dispersion polymerization.[59, 62-63] Such nanoparticles exhibit sufficient surface activity to stabilize both Pickering macroemulsions[59, 64] and nanoemulsions.[36, 48] Furthermore, such nanoparticles can be prepared in water,[59, 61-62, 65-68] polar solvents (e.g. lower alcohols)[60, 69-77] and non-polar solvents (e.g. *n*-alkanes[78-86] or mineral oil[82, 87]). Thus they are suitable for the preparation of o/w,[59, 88] o/o[89-90] and w/o[91-92] emulsions. For example, Thompson et al.[48] recently reported that 25 nm diameter diblock copolymer nanoparticles can be used in combination with high-pressure microfluidization to produce o/w Pickering nanoemulsions. Subsequently, the effect of varying the *n*-alkane oil phase on the long-term stability of such nanoemulsions was examined.[36] Analytical centrifugation proved to be the most useful sizing technique for monitoring droplet coarsening over time. Pickering nanoemulsions prepared using either *n*-octane or *n*-decane proved to be significantly less stable towards Ostwald ripening than those prepared with either *n*-dodecane or *n*-tetradecane. This difference was rationalized in terms of the significantly higher aqueous solubility of the former pair of *n*-alkanes. In a follow-up study, Hunter et al. found that introducing terminal anionic or cationic charge at the end of the steric

stabilizer chains is detrimental to both the adsorption efficiency of the diblock copolymer nanoparticles and also the long-term stability of the Pickering nanoemulsions.[53]

Herein we report the production of relatively stable w/o Pickering nanoemulsions using bespoke diblock copolymer nanoparticles prepared via RAFT dispersion polymerization in *n*-dodecane. This is achieved by first preparing a w/o Pickering macroemulsions via conventional high-shear homogenization using a large excess of nanoparticles, followed by high-pressure microfluidization to generate the desired w/o Pickering nanoemulsion. Such nanoemulsions are complementary to the o/w Pickering nanoemulsions previously reported by Thompson and co-workers.[36, 48] The effect of systematically increasing the concentration of added salt within the dispersed phase on the z-average diameter of the aqueous droplets is examined. Subsequently, the effect of varying the initial nanoparticle concentration, the number of passes through a high-pressure microfluidizer and the applied pressure during microfluidization on the final nanoemulsion droplet diameter is investigated. Finally, the effect of varying the amount of salt dissolved in the aqueous dispersed phase on the long-term stability of these w/o Pickering nanoemulsions is explored.

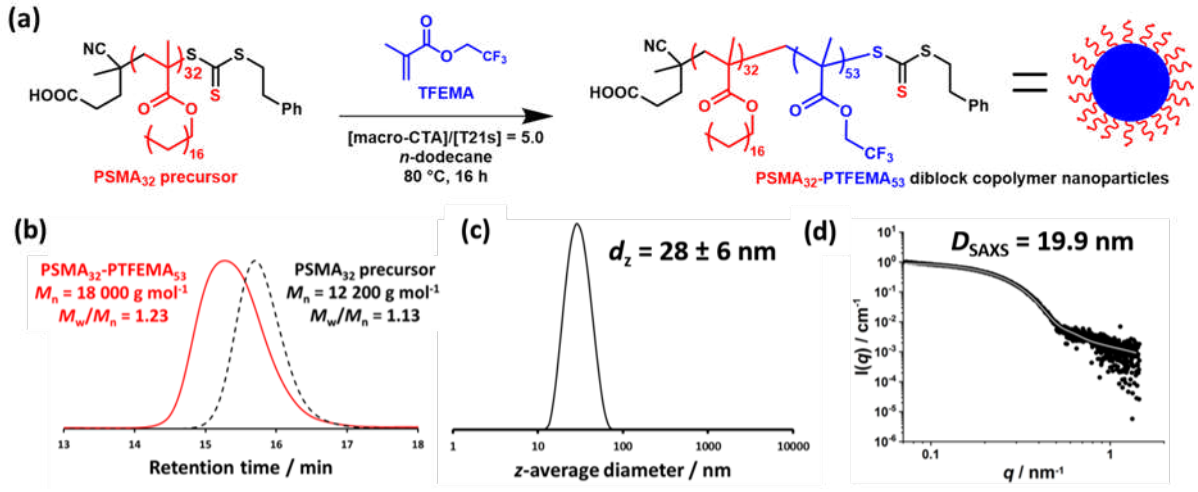

Figure 1. (a) Synthesis of $PSMA_{32}$–$PTFEMA_{53}$ nanoparticles via RAFT dispersion polymerization of TFEMA at 80 °C using a $PSMA_{32}$ precursor; (b) overlaid DMF GPC curves obtained for a $PSMA_{32}$ precursor and the corresponding $PSMA_{32}$-$PTFEMA_{53}$ diblock copolymer; (c) intensity-average particle size distribution determined by DLS; (d) Experimental SAXS pattern (black circles) recorded for a 1.0% w/w dispersion of $PSMA_{32}$-$PTFEMA_{53}$ diblock copolymer nanoparticles in *n*-dodecane. A satisfactory data fit was obtained using a spherical micelle model (white line), see Supporting Information.

EXPERIMENTAL

Materials. Stearyl methacrylate (SMA), 2,2,2-trifluoroethyl methacrylate (TFEMA), *n*-dodecane, trimethylamine, butylhydroxytoluene (BHT) tetrahydrofuran (THF), toluene, 2,2-azobis(2-methylpropionitrile) (AIBN), lauroyl peroxide (Luperox®), ruthenium(IV) oxide hydrate and sodium periodate were all purchased from Sigma-Aldrich (UK). Monomers were passed through basic alumina in order to remove inhibitor prior to use. Tert-Butyl peroxy-2-ethylhexanoate (Trigonox 21S, or T21s) initiator was supplied by AkzoNobel (The Netherlands). *d*-Chloroform ($CDCl_3$) was purchased from VWR (UK), d_2-dichloromethane (CD_2Cl_2) was obtained from Cambridge Isotope Laboratory (USA) and the 4-cyano-4-((2-phenylethanesulfonyl)thiocarbonylsulfanyl)pentanoic acid (PETTC) RAFT agent was prepared in-house according to a previously reported protocol.[93] Unless stated otherwise, deionized water (pH 6) was used for all experiments.

Synthesis of a $PSMA_{32}$ precursor via RAFT solution polymerization. A $PSMA_{32}$ precursor was prepared via RAFT solution polymerization of SMA in toluene using a trithiocarbonate-based PETTC RAFT agent, as previously described.[94] The reaction solution was heated by immersing the flask in an oil bath set at 70 °C and the resulting SMA polymerization was quenched by exposure to air after 4 h. ^{1}H NMR analysis in CD_2Cl_2 indicated 83% SMA conversion under these conditions. A mean DP of 32 was determined via ^{1}H NMR analysis in CD_2Cl_2; the integrated aromatic PETTC signals at 7.1–8.1 ppm were compared to that of the oxymethylene signal at 3.7–4.2 ppm. This analysis indicated a RAFT agent efficiency of 96%. THF GPC studies (refractive index detector; using a series of eight near-monodisperse polymethyl methacrylate calibration standards) indicated an M_n of 12 300 g mol^{-1} and an M_w/M_n of 1.13.

Synthesis of $PSMA_{32}$-$PTFEMA_{53}$ diblock copolymer nanoparticles via RAFT dispersion polymerization of TFEMA. The synthesis of $PSMA_{32}$-$PTFEMA_{53}$ spheres at 20% w/w solids was conducted as follows: a $PSMA_{32}$ precursor (2.01 g, 0.18 mmol), lauroyl peroxide (77 mg, 0.036 mmol), and *n*-dodecane (14.6 g, 19.5 ml) were added in turn to a glass vial and the resulting solution was degassed with N_2 gas for 30 min at 20 °C. TFEMA was degassed separately in ice to minimize evaporation. This monomer (1.95 ml, 9.82 mmol; target DP = 55) was then added via syringe to the reaction mixture, which was subsequently heated to 80 °C for 16 h by immersing the vial in an oil bath. ^{19}F NMR spectroscopy analysis of the copolymer dissolved in $CDCl_3$ indicated 97% TFEMA conversion under these conditions. THF GPC studies (refractive index detector; using a series of eight near-monodisperse polymethyl methacrylate calibration standards) indicated an M_n of 18 000 g mol^{-1} and an M_w/M_n of 1.23

Preparation of $PSMA_{32}$-$PTFEMA_{53}$-stabilized Pickering macroemulsions using high-shear homogenization. A 5.0% w/w dispersion of $PSMA_{32}$-$PTFEMA_{53}$ nanoparticles in *n*-dodecane (4.5 mL) was added to a 14 mL glass vial. This was then homogenized with various aqueous solutions (prepared using deionized water at around pH 6, unless stated otherwise) (0.5 mL; containing 0-0.43 M NaCl) for 2 min at 20 °C using an IKA Ultra-Turrax T-18 homogenizer equipped with a 10 mm dispersing tool and operating at 13 500 rpm.

Preparation of $PSMA_{32}$-$PTFEMA_{53}$-stabilized Pickering Nanoemulsions using high-pressure microfluidization. A Pickering macroemulsion (5.0 mL, initial nanoparticle concentration in the *n*-dodecane phase = 5.0% w/w) was further processed using an LV1 microfluidizer (Microfluidics, USA). The pressure was fixed at 10 000 psi and each emulsion was passed five times through the LV1 unit to produce unimodal w/o Pickering nanoemulsions.

THF GPC. Molecular weight distributions were assessed by gel permeation chromatography (GPC) using THF as an eluent. The GPC set-up comprised an Agilent 1260 Infinity series degasser and pump, two Agilent PLgel 5 μm Mixed C columns in series and a refractive index

detector. The mobile phase contained 2.0% v/v trimethylamine and 0.05% w/w butylhydroxytoluene (BHT) and the flow rate was fixed at 1.0 ml min^{-1}. Copolymer samples were dissolved in THF containing 0.50% v/v toluene as a flow-rate marker prior to GPC analysis. A series of eight near-monodisperse polymethyl methacrylate standards (M_p values ranging from 580 to 552 500 g mol^{-1}) were used for calibration using either a refractive index detector or a UV detector operating at 260 nm.

NMR spectroscopy. ^{19}F NMR spectra were recorded in $CDCl_3$ using a Bruker Avance III HD spectrometer operating at 400.23 MHz (^1H frequency). Spectra were recorded using 16 transients with an acquisition window of 89.3 kHz, 128 points and a relaxation delay of 1 s. Spectra were analyzed using TopSpin version 3.1 software. TFEMA conversions were determined by comparing the integrated intensities of signals assigned to residual monomer and the corresponding polymer.

Transmission Electron Microscopy (TEM). The staining agent was prepared by dissolving ruthenium(IV) oxide hydrate (0.30 g) and sodium periodate (2.00 g) in 50 ml water. The copolymer dispersion was diluted to 0.1% w/w in *n*-dodecane and a single droplet was placed on a carbon-coated copper TEM grid with the aid of a micropipet. The loaded grid was stained for 7 min by exposure to the heavy metal stain within a desiccator. TEM images were recorded using a Tecnai Spirit T12 TEM instrument operating at 80 kV and equipped with an Orius SC1000B S4 CCD camera (2672 x 4008 pixels; 9 μm each).

Scanning electron microscopy (SEM). The copolymer dispersion was diluted to 1% v/v using *n*-dodecane and one droplet was placed on a glass slide, which was then left to dry overnight. The glass slide was then mounted onto an SEM stub using an electrically conductive adhesive pad. The stub was gold-coated for 2 min prior to analysis. SEM studies were performed using an Inspect F field emission microscope operating at 5 kV.

Dynamic Light Scattering (DLS). Intensity-average hydrodynamic diameters were obtained by DLS using a Malvern Zetasizer NanoZS instrument at a fixed scattering angle of 173°. Dispersions of 0.1% w/w nanoemulsions were analyzed using disposable cuvettes, and the results were averaged over three consecutive runs, each comprising ten analyses. The *n*-dodecane used to dilute each sample was ultrafiltered through a 0.20 μm membrane to remove extraneous dust.

Analytical Centrifugation (LUMiSizer). Aqueous droplet size distributions were assessed using a LUMiSizer analytical photocentrifuge (LUM GmbH, Berlin, Germany) at 20 °C. Measurements were conducted on diluted Pickering nanoemulsions (1.0-10.0% v/v water) using 2 mm pathlength polyamide cells at 400 rpm for 200 profiles (allowing 10 s between profiles) and then the rate of centrifugation was increased up to 4000 rpm for a further 800 profiles The slow initial rate of centrifugation enabled detection of any larger oil droplets that might be present within the nanoemulsion. Overall, the measurement time is approximately 135 min. The LUMiSizer instrument employs space- and time-resolved extinction profiles (STEP) technology to measure the intensity of transmitted near-infrared light as a function of time and position simultaneously over the entire length of the cell. The gradual progression of these transmission profiles provides information on the rate of sedimentation of the aqueous droplets and hence enables assessment of the droplet size distribution. The particle density is an essential input parameter for analytical centrifugation studies. The droplet density used for the nanoemulsion ageing studies was either the density of pure water or the appropriate density for a given aqueous salt solution (which is 1.016 g cm^{-3} for the highest NaCl concentration (0.43 M) used in this study).[95] This ignores any contribution to the droplet density from the adsorbed $PSMA_{32}$-$PTFEMA_{53}$ nanoparticles, but this approximation is reasonable given that we merely wish to assess *relative* changes in the droplet size distribution over time.

Small-Angle X-ray Scattering. Small-angle X-ray scattering (SAXS) patterns were recorded using a laboratory SAXS beamline (Xeuss 2.0, Xenocs, France) equipped with a liquid gallium MetalJet X-ray source (Excillum, Sweden) (wavelength λ = 0.134 nm), two sets of motorized scatterless slits for beam collimation, and a Pilatus 1M two-dimensional pixel SAXS detector (Dectris, Switzerland). A flow-through glass capillary (2 mm diameter) was connected to an injector syringe and a waste container via plastic tubing and mounted horizontally on the beamline stage; this set-up was used as a sample holder. SAXS patterns were recorded over a q range of 0.01−1.4 nm^{-1}, where $q = (4\pi \sin\theta)/\lambda$ is the length of the scattering vector, and θ is a half of the scattering angle. Two-dimensional SAXS patterns were reduced to one-dimensional curves using the Foxtrot software package supplied with the instrument and further analyzed (background subtraction and data modeling) using Irena SAS macros[96] for Igor Pro.

Packing efficiency calculation

The nanoparticle packing efficiency was estimated by first calculating the number of nanoparticles, N, adsorbed onto an individual aqueous droplet using equation 1:[36]

$$N = \frac{\text{total number of nanoparticles}}{\text{total number of droplets}} = \frac{m_{\text{particles}} N_A / N_s M_n}{V_{\text{water}} / \left(\frac{4}{3}\pi R_{\text{water}}\right)^3} \quad (1)$$

where it is assumed that all nanoparticles are adsorbed at the water-oil interface. Here, $m_{\text{particles}}$ is the mass of nanoparticles used to prepare the nanoemulsion, N_A is Avogadro's constant, M_n is the number−average molecular weight of the $PSMA_{32}$−$PTFEMA_{53}$ chains, V_{water} is the total volume of water used to prepare each nanoemulsion, and R_{water} is the average radius of bare aqueous droplets. Finally, N_s is the number of $PSMA_{32}$−$PTFEMA_{53}$ chains per nanoparticle determined as $N_s = \frac{\frac{4}{3}\pi R_s^3}{V_{\text{PTFEMA}}}$ where R_s is the mean radius of the PTFEMA cores measured by SAXS and V_{PTFEMA} is volume of the core-forming block of a copolymer molecule. We calculate R_{water} to be equal to the z-average radius (R_{DLS}) of the overall nanoemulsion droplets minus the

diameter of the adsorbed nanoparticles (or $R_{water} = R_{DLS} - 2R_{particle}$). The volume-average diameter of the nanoparticles could be calculated from SAXS measurements of the nanoparticles as $2R_s + 4R_g$, where R_g is radius of gyration of the micelle $PSMA_{32}$ corona block. However, we contend that the *effective* diameter ($2R_{particle}$) of the $PSMA_{32}$–$PTFEMA_{53}$ nanoparticles adsorbed at the oil-water interface is actually given by $2R_s + 2R_g$.[36] This is because the non-solvated $PSMA_{32}$ stabilizer chains that are in direct contact with the aqueous phase most likely adopt a fully collapsed conformation and hence occupy negligible volume at the oil-water interface.

Assuming that an area of a large spherical particle covered by small spheres can be represented by the total area of projections of the small spheres on the large particle surface,[97] the packing efficiency, P, of the small spheres in the large particle shell is given by equation 2:

$$P \cong \frac{N(R_{particle})^2}{4(R_{water}+R_{particle})^2} \quad (2)$$

We make the following assumptions in our nanoparticle packing efficiency calculations. First, the z-average droplet diameter reported by DLS includes both the oil droplet and the adsorbed nanoparticle shell. Secondly, the nanoparticles adsorb at the oil-water interface with an effective contact angle of 0° with respect to the nanoparticle cores. Clearly, this is not the true nanoparticle contact angle, hence the droplet diameter will be slightly overestimated. Finally, since we assume that all of the nanoparticles adsorb at the surface of the aqueous droplets, the calculated nanoparticle packing efficiency should be regarded as an upper limit value as some minor fraction of nanoparticles could remain within the continuous phase.

RESULTS AND DISCUSSION

The sterically-stabilized diblock copolymer nanoparticles used in this study were prepared by chain-extending an oil-soluble poly(stearyl methacrylate) (PSMA) precursor with 2,2,2-trifluoroethyl methacrylate (TFEMA), as previously described by Cornel and co-workers (see Figure 1a).[94] Provided that a relatively short PTFEMA block of 55 is targeted, this PISA formulation enables the preparation of PTFEMA-core spherical nanoparticles with a mean diameter of less than 30 nm,[94] which is expected to be sufficiently small for the production of Pickering nanoemulsions.[35, 48] ^{19}F NMR spectroscopy studies indicated that the TFEMA polymerization proceeded to relatively high monomer conversion (~97%) within 16 h at 80 °C (see Figure S1). GPC analysis (THF eluent) indicated a relatively narrow molecular weight distribution (M_w/M_n = 1.23), suggesting that this RAFT dispersion polymerization was well-controlled (see Figure 1b). The intensity-average diameter of the sterically-stabilized nanoparticles determined by DLS is 28 ± 6 nm (Figure 1c), which is consistent with the number-average diameter of 24 ± 4 nm estimated from TEM analysis (based on analysis of more than 100 nanoparticles) (Figure 6d. The SAXS pattern recorded for these nanoparticles was fitted using a spherical micelle form factor.[98] This approach indicated a mean PTFEMA core radius (R_s) of 6.5 nm (and an associated standard deviation, σ_s, of 1.3 nm) and a radius of gyration (R_g) for the PSMA corona block of 1.72 nm, resulting in a volume-average diameter ($2R_s + 4R_g$) of 19.9 nm (see Figure 1e and the Supporting Information for further details of the scattering model). This is somewhat smaller than the nanoparticle dimensions indicated by DLS and TEM. However, DLS reports a hydrodynamic diameter while TEM analysis suffers from poor statistics, so both techniques overestimate the effective particle dimensions indicated by SAXS.

Such $PSMA_{32}$-$PTFEMA_{53}$ nanoparticles were used to prepare a precursor Pickering macroemulsion of approximately 10-20 µm diameter via high-shear homogenization using an Ultra-Turrax homogenizer (see Figure 2). A water volume fraction of 0.10 and a nanoparticle concentration of 5.0% w/w was used to prepare this macroemulsion. These conditions were deliberately selected because a substantial excess of non-adsorbed nanoparticles is required to stabilize the substantial increase in interfacial area that is generated during the subsequent high-pressure microfluidization to produce the much finer Pickering nanoemulsion.[35, 48]

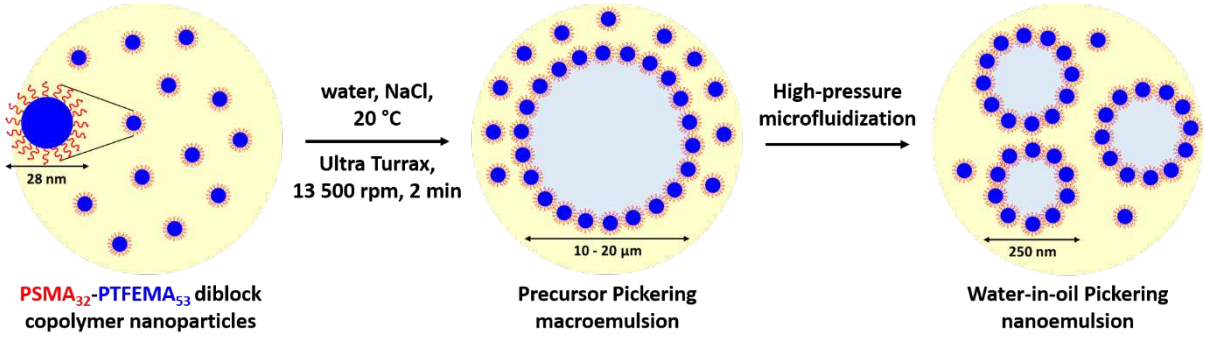

Figure 2. Schematic representation of the preparation of water-in-oil (w/o) Pickering nanoemulsions reported in this study. A precursor Pickering macroemulsion was prepared using high-shear homogenization, and then further processed using the LV1 microfluidizer to produce a w/o Pickering nanoemulsion. A large excess of non-adsorbed nanoparticles co-exist with the macroemulsion but very few non-adsorbed nanoparticles remain in the continuous phase after high-pressure microfluidization.

In initial microfluidization experiments no salt was added to the aqueous phase. A precursor macroemulsion prepared using 5.0% w/w $PSMA_{32}$-$PTFEMA_{53}$ nanoparticles was subjected to repeated passes through an LV1 microfluidizer at various applied pressures, with the mean droplet diameter being assessed by DLS after each pass. At an applied pressure of 5000 psi, the mean droplet diameter was reduced significantly between the first and tenth pass (Figure S2). However, there was no further change when using higher applied pressures (e.g., 10 000 or 20 000 psi) and *larger* droplets were observed at 30 000 psi owing to over-shearing. The mean droplet diameters for such emulsions exceeded 600 nm, which is significantly greater than those reported by Thompson and co-workers for o/w nanoemulsions prepared using

$PGMA_{48}$-$PTFEMA_{50}$ diblock copolymer nanoparticles.[36, 48] Moreover, such coarse droplets do not correspond to genuine nanoemulsions, which should be less than 200 nm diameter.[32]

One of the reviewers of this manuscript suggested that ionization of the carboxylic acid end-groups on the $PSMA_{32}$ stabilizer chains might occur at the *n*-dodecane-water interface. To examine this hypothesis, we prepared two Pickering nanoemulsions using an aqueous 0.11 M NaCl solution adjusted to either pH 7 or pH 2. In the former case, the formation of anionic carboxylate groups at the *n*-dodecane-water interface was anticipated, whereas in the latter case no such ionization should occur. DLS studies of the nanoemulsion at pH 7 indicated a droplet diameter of 268 ± 96 nm, which is comparable to the nanoemulsion using deionized water at pH 6 (see entry 2 in Table 1). On the other hand, the Pickering nanoemulsion prepared at pH 2 had a droplet diameter of 217 ± 92 nm, see Figure S3. These observations indicate that ionization of the carboxylic acid end-groups on the steric stabilizer chains of these nanoparticles leads to the formation of a slightly larger nanoemulsion than that formed when using neutral nanoparticles. We have recently made similar observations for a closely-related *n*-dodecane-in-water Pickering nanoemulsion.[53] However, further work would be required to establish whether such end-group ionization also affected the nanoparticle adsorption efficiency, the nanoparticle packing efficiency at the oil-water interface, and the long-term stability of such nanoemulsions.

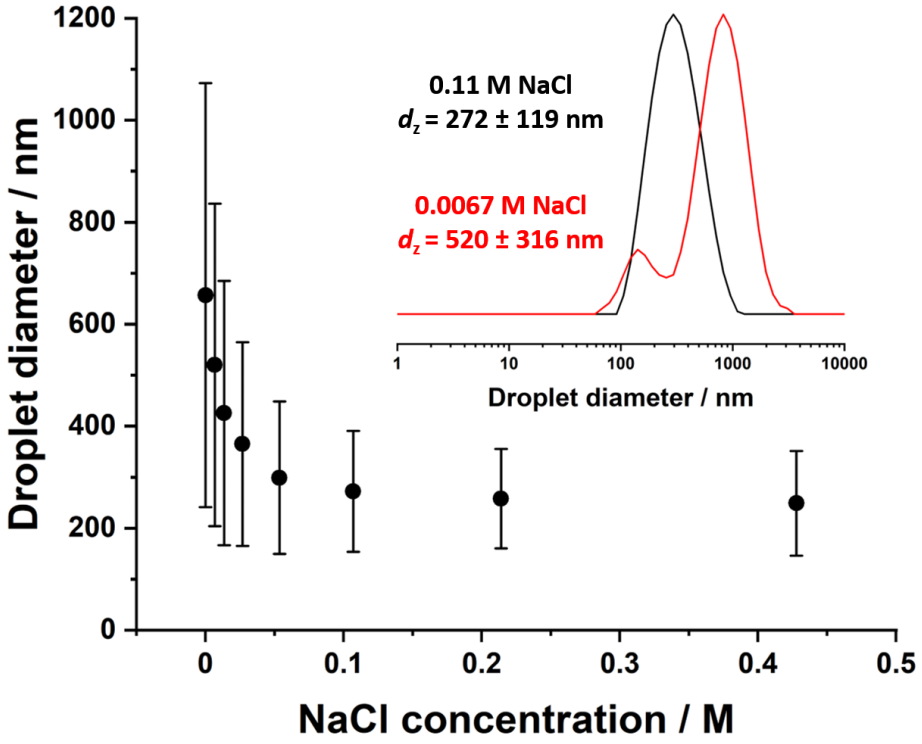

Figure 3. Systematic reduction in intensity-average droplet diameter observed for a w/o Pickering nanoemulsion prepared at a water volume fraction of 0.10 using 5.0% w/w $PSMA_{32}$-$PTFEMA_{53}$ nanoparticles in *n*-dodecane while varying the NaCl concentration. Error bars represent the standard deviation of the droplet size distributions, rather than the experimental error associated with repeated measurements. Inset: intensity-average droplet size distributions determined by DLS for Pickering nanoemulsions prepared with either 0.11 M or 0.0067 M NaCl dissolved within the aqueous phase (deionized water at pH 6).

In the case of surfactant-stabilized w/o nanoemulsions, it is well-known that addition of electrolyte to the aqueous phase prior to emulsification results in the formation of smaller, more stable droplets.[22, 99] Therefore, aqueous solutions containing up to 0.43 M NaCl were used to prepare w/o Pickering nanoemulsions using 5.0% w/w $PSMA_{32}$-$PTFEMA_{53}$ nanoparticles at an applied pressure of 10 000 psi with 5 passes through the LV1 microfluidizer. Figure 3 shows the effect of varying the NaCl concentration on the mean droplet diameter, as indicated by DLS studies. The droplet diameter and polydispersity index are both reduced significantly at higher salt concentrations. A limiting droplet diameter of around 250 nm is achieved at 0.43 M NaCl. This *overall* diameter necessarily includes the thickness of the adsorbed $PSMA_{32}$–$PTFEMA_{53}$ nanoparticle layer. If this nanoparticle contribution is subtracted, the mean diameter for the underlying 'naked' aqueous droplet is less than 200 nm, which meets the criterion for a

nanoemulsion according to the literature.[13] Below the critical concentration of 0.11 M MaCl, visual inspection confirmed that coarser nanoemulsion droplets sediment on standing overnight at 20 °C (see Figure S4). Moreover, bimodal droplet size distributions are observed for such nanoemulsions. In contrast, nanoemulsions possess unimodal droplet size distributions when prepared in the presence of at least 0.11 M NaCl and do not undergo sedimentation under the same conditions.

In order to assess whether high-pressure microfluidization may induce nanoparticle dissociation or degradation, a control experiment was performed in which a 5.0% w/w dispersion of $PSMA_{32}$-$PTFEMA_{53}$ nanoparticles in *n*-dodecane was subjected to the above optimized processing conditions (applied pressure = 10 000 psi, number of passes = 5) *in the absence of any aqueous solution*. DLS studies conducted before and after microfluidization confirmed that the z-average diameter of the nanoparticles (and DLS polydispersity) remained essentially unchanged (data not shown). Thus the $PSMA_{32}$-$PTFEMA_{53}$ nanoparticles survive the high-pressure microfluidization conditions intact.

Table 1. Summary of Droplet Density, Droplet Diameter, Number of Nanoparticles Per Droplet and Packing Efficiency for four Pickering Nanoemulsions Prepared Using 5.0% w/w $PSMA_{32}$-$PTFEMA_{53}$ Diblock Copolymer Nanoparticles with 0.05 M to 0.43 M NaCl Dissolved in the Aqueous Phase.

NaCl concentration / M	Aqueous droplet density / g cm^{-3}	Initial DLS droplet diameter / nm	Number of nanoparticles per droplet, *N*	Packing efficiency, *P* / %
0.05	1.0003	299 ± 150	362	75
0.11	1.003	272 ± 119	257	66
0.21	1.007	258 ± 97	211	61
0.43	1.016	249 ± 103	185	58

The mean packing efficiency for the adsorbed layer of nanoparticles surrounding each aqueous droplet was calculated for fresh Pickering nanoemulsions prepared in the presence of added salt (0.05 M to 0.43 M NaCl) (Table 1) using a core-shell model originally developed by Balmer et al. to study the adsorption of 20 nm silica nanoparticles onto large polymer latexes.[97]

This model was recently applied to oil-in-water Pickering nanoemulsions by Thompson et al.[36] For the latter system, an effective contact angle of 0° was assumed for nanoparticle adsorption at the oil-water interface and the same assumption was made in the present study. Increasing the NaCl concentration within the aqueous phase leads to a higher droplet density and a gradual reduction in the intensity-average droplet diameter, as expected. This size reduction necessarily reduces the number of spheres per droplet but the nanoparticle packing efficiency is also significantly reduced from 75% to 58% on raising the NaCl concentration from 0.05 M to 0.43 M NaCl. One possible explanation for this reduction in packing efficiency might be a lower three-phase particle contact angle, θ, in the presence of additional salt. In principle, the hydrophobic $PSMA_{32}$-$PTFEMA_{53}$ nanoparticles adsorbed at the surface of the aqueous droplets should exhibit poorer wettability at higher NaCl concentrations.

The packing efficiencies calculated herein are broadly comparable to those determined by Thompson et al. for *n*-dodecane-in-water Pickering nanoemulsions, which were stabilized using hydrophilic 25 nm $PGMA_{48}$-$PTFEMA_{50}$ diblock copolymer nanoparticles prepared via RAFT aqueous emulsion polymerization.[36] More specifically, in this prior study the number of adsorbed nanoparticles per droplet, N, and the packing efficiency, P, were calculated to be 438 and 74% for *n*-dodecane droplets with a z-average diameter of 257 ± 93 nm. In the present study, a water-in-oil Pickering nanoemulsion prepared with a similar mean droplet diameter using 0.21 M NaCl at pH 6 had $N = 211$ and $P = 61\%$, respectively (see entry 3 in Table 1).

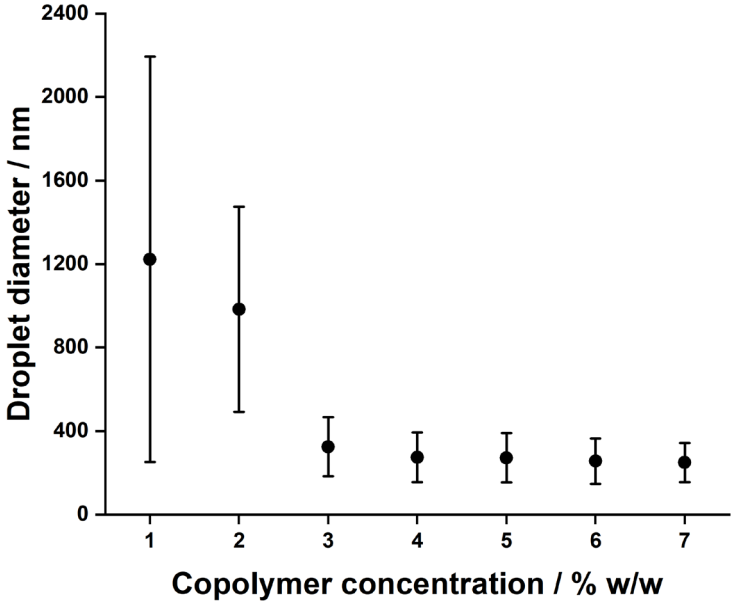

Figure 4. Variation in the intensity-average aqueous droplet diameter with nanoparticle concentration for w/o Pickering nanoemulsions prepared using $PSMA_{32}$-$PTFEMA_{53}$ nanoparticles after five passes through an LV1 microfluidizer. Conditions: water volume fraction = 0.10; 0.11 M NaCl; applied pressure = 10 000 psi. Errors bars represent standard deviations for the DLS droplet size distributions, rather than the experimental error associated with repeated measurements.

The $PSMA_{32}$-$PTFEMA_{53}$ nanoparticle concentration was systematically varied at a fixed 0.11 M NaCl, which corresponds to the minimum salt concentration required to prepare well-defined Pickering nanoemulsion droplets with a z-average diameter of 274 ± 119 nm. A significant reduction in the mean droplet diameter was observed when increasing the nanoparticle concentration from 1.0 to 4.0% w/w (see Figure 4). However, preparing nanoemulsions under the same conditions using higher nanoparticle concentrations (up to 7.0% w/w) did not result in a further reduction in droplet size. Such behavior is typical for Pickering nanoemulsions and have been previously reported when using other particulate emulsifiers.[35, 48, 50, 56, 100] This provides strong (albeit indirect) evidence that the $PSMA_{32}$-$PTFEMA_{53}$ nanoparticles survive the high-pressure microfluidization required to generate nano-sized droplets. Moreover, the mean droplet diameter reaches a minimum value at a copolymer concentration of 4.0% w/w. Assuming that all the nanoparticles are adsorbed onto the aqueous droplets and an effective nanoparticle density of approximately 1 g cm^{-3}, we estimate that N = 211 and P = 53% under such conditions. Such values seem to be physically reasonable given

the data reported in Table 1. Thus. the initial limiting droplet diameter appears to correspond to maximum overall efficiency: i.e. the smallest possible aqueous droplets coated with all (or almost all) of the nanoparticles present in the formulation.

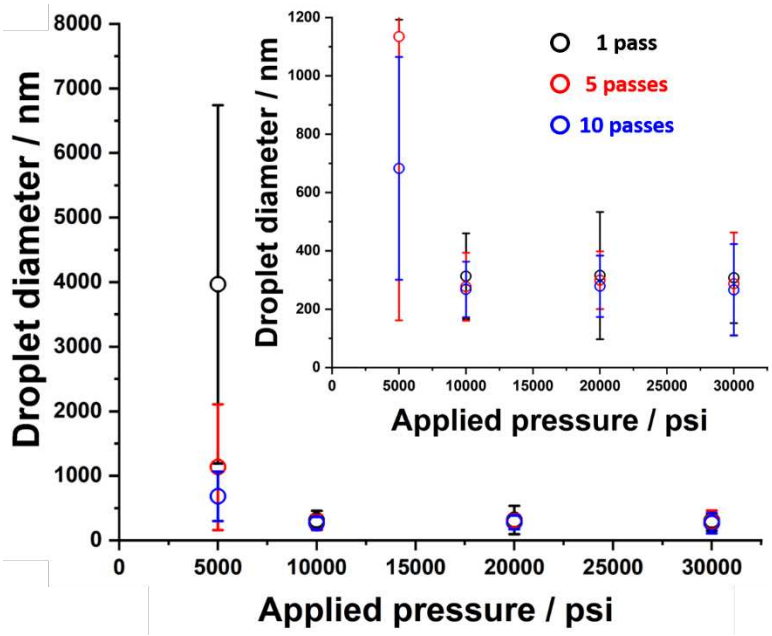

Figure 5. Variation in the intensity-average droplet diameter with applied pressure when preparing w/o Pickering nanoemulsions using an LV1 microfluidizer with 1, 5 or 10 pass(es). Conditions: water volume fraction = 0.10; 5.0% w/w $PSMA_{32}$-$PTFEMA_{53}$ nanoparticles; 0.11 M NaCl. Error bars represent standard deviations for the DLS droplet size distributions, rather than the experimental error associated with repeated measurements. The data shown in the inset are replotted over a narrower range of droplet diameters for the sake of clarity.

A precursor w/o Pickering macroemulsion prepared using 5.0% w/w $PSMA_{32}$-$PTFEMA_{53}$ nanoparticles was subjected to up to 10 passes through the LV1 microfluidizer at various applied pressures. The mean droplet diameter was assessed using DLS after 1, 5 and 10 passes (see Figure 5). At 5 000 psi, a significant reduction in emulsion droplet diameter was observed between the first and tenth passes. When the applied pressure was raised to 10 000 psi, the mean droplet diameter was reduced from 683 ± 382 nm to 268 ± 95 nm. However, for applied pressures ranging from 10 000 to 30 000 psi, only rather subtle changes in the mean droplet diameter were observed. Furthermore, only modest changes in droplet diameter were observed after each pass. In view of these empirical observations, an applied pressure of 10 000 psi and 5 passes was used to prepare w/o Pickering nanoemulsions in all subsequent experiments.

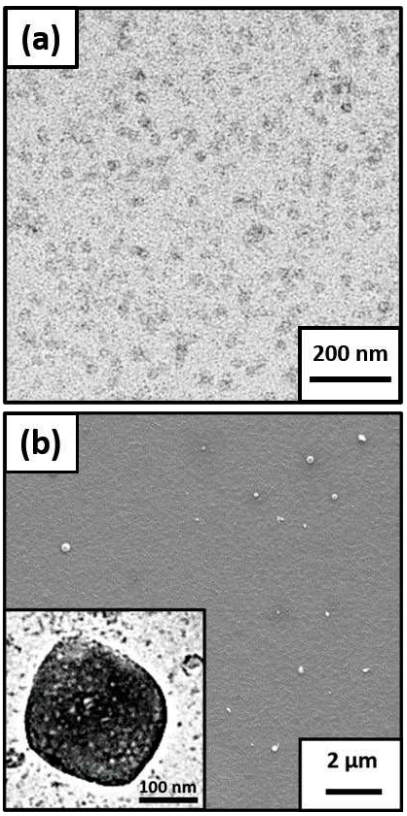

Figure 6. (a) TEM image recorded for a dried dilute dispersion of sterically stabilized $PSMA_{32}$–$PTFEMA_{53}$ nanoparticles. (b) Representative SEM and (inset) TEM images recorded for dried water-in-*n*-dodecane Pickering nanoemulsions prepared using 5.0% w/w $PSMA_{32}$-$PTFEMA_{53}$ nanoparticles with 0.11 M NaCl dissolved in the aqueous phase. Conditions: microfluidization pressure = 10 000 psi; 5 passes.

A w/o Pickering nanoemulsion was prepared under optimized conditions (10 000 psi, 5 passes, 5.0% w/w $PSMA_{32}$-$PTFEMA_{53}$ nanoparticles) to visualize the remnants of dried droplets (i.e. the remaining nanoparticle superstructure) using TEM and SEM studies. Representative TEM images are shown in Figure S5. As expected, the number-average droplet diameter of 168 ± 73 nm (estimated from analysis of 50 droplets) is somewhat lower than the z-average diameter reported by DLS (272 ± 119 nm). On close inspection (see inset), it is clear that the spherical nanoparticles have survived the high-pressure microfluidization conditions intact. Thus the w/o nanoemulsion is a genuine Pickering nanoemulsion, rather than simply a nanoemulsion that is stabilized by molecularly-dissolved diblock copolymer chains acting as a polymeric surfactant. This was not unexpected, because the $PSMA_{32}$ and $PTFEMA_{53}$ blocks are both hydrophobic, so the diblock copolymer chains do not possess any amphiphilic character. SEM images

recorded for the same nanoemulsion also indicated that spherical aqueous droplets were produced (see Figure 6).

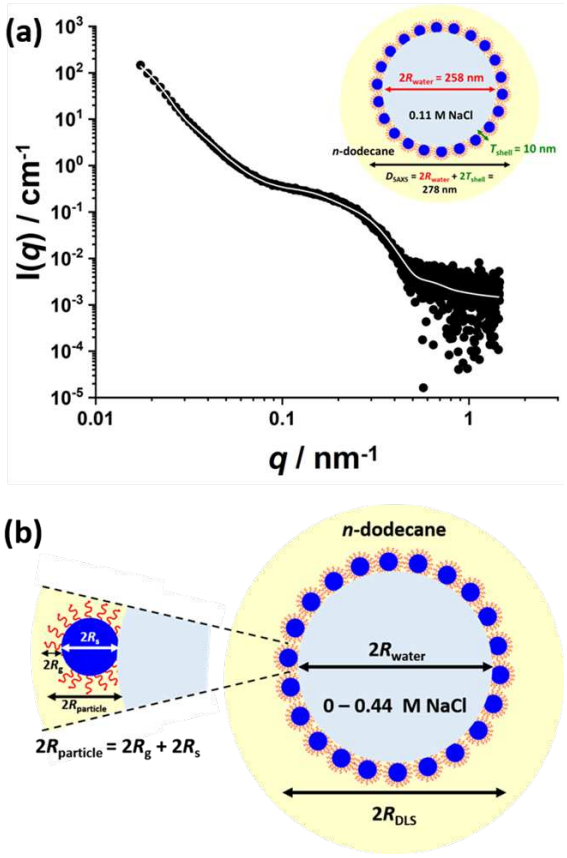

Figure 7. (a) SAXS pattern (circles) and corresponding data fit (white line) obtained for a 1.0% v/v Pickering nanoemulsion prepared using 5.0% w/w $PSMA_{32}$-$PTFEMA_{53}$ nanoparticles and an aqueous phase containing 0.11 M NaCl and adjusted to pH 6. This nanoemulsion was prepared using an LV1 microfluidizer at an applied pressure of 10 000 psi for 5 passes. The two-population core−shell structural model used for the SAXS analysis of this Pickering nanoemulsion comprises aqueous droplet cores coated with an adsorbed layer of $PSMA_{32}$-$PTFEMA_{53}$ spherical nanoparticles. (b) Schematic representation of the adsorption of such nanoparticles at the *n*-dodecane/water interface. It is assumed that (i) these nanoparticles are adsorbed with an effective contact angle of 0° and (ii) $PSMA_{32}$ stabilizer chains in direct contact with the *n*-dodecane/water interface are fully collapsed and hence do not contribute to the adsorbed nanoparticle radius. Thus, given that the effective thickness of these adsorbed sterically-stabilized nanoparticles is given by $2R_s + 2R_g$ (rather than $2R_s + 4R_g$), the approximate effective sphere radius, $R_{particle}$, is given by $R_{particle} = R_s + R_g = 8.2$ nm. Experimental values for R_s and R_g were obtained from SAXS analysis of the $PSMA_{32}$−$PTFEMA_{53}$ nanoparticles prior to emulsification, see the main text.

To determine the mean thickness of the nanoparticles adsorbed at the surface of the aqueous droplets, a SAXS pattern was recorded for a freshly-prepared Pickering nanoemulsion immediately after dilution to 1.0% v/v (Figure 7). Following our recent study of the characterization of complementary *n*-dodecane-in-water Pickering nanoemulsions,[53] this SAXS pattern was analyzed using a two-population model (see the Supporting Information). One of the populations (population 2) is represented by core−shell spheres, where the core

comprises the aqueous droplet and the shell is composed of an adsorbed monolayer of spherical micelles. The particulate nature of the shell is described by the spherical micelles with a hard-sphere structure factor to account for inter-particle interactions at the oil-water interface, which corresponds to population 1. In order to minimize the number of fitting parameters, the mean micelle core radius (R_s) and its associated standard deviation (σ_s) determined by analysis of the nanoparticles alone (Figure 1e) were used and these values were held constant when analyzing the SAXS pattern of the Pickering nanoemulsion using the two-population model. The scattering length density for each component of the Pickering nanoemulsion [aqueous droplet core (ξ_{core} = 9.42 × 10^{10} cm^{-2}), particulate shell (ξ_{shell} = 10.34 × 10^{10} cm^{-2}, see the Supporting Information), and the *n*-dodecane continuous phase (ξ_{sol} = 7.63 × 10^{10} cm^{-2})] was calculated based on their respective chemical compositions and mass densities. These three parameters were also fixed for the subsequent data fit to the SAXS pattern recorded for the Pickering nanoemulsion, whose structure can be described by the mean core radius (R_c) and its standard deviation (σ_c), the mean shell thickness (T_{shell}), and two scaling factors (volume fraction φ_1 for population 1 and volume fraction φ_2 for population 2, see Supporting Information). Two additional parameters were required to account for the packing of spherical micelles at the surface of the aqueous droplets: the micelle interaction radius, R_{PY}, and the effective volume fraction, f_{PY} (Equation *S8*). These seven parameters were used to fit the SAXS data (Figure 7).

The shape of the SAXS pattern (Figure 7) is similar to that previously reported for *n*-dodecane-in-water Pickering nanoemulsions prepared using hydrophilic $PGMA_{48}$-$PTFEMA_{50}$ nanoparticles.[53] Three main regions can be discerned: (i) relatively intense scattering at low q arising from the nanoemulsion droplets (close inspection reveals a subtle change in the gradient at low q, indicating cross-over from the Guinier region to the Porod region); (ii) additional scattering intensity at intermediate q corresponding to the nanoparticle form factor (see Figure 1e); (iii) relatively weak scattering at high q, which is associated with both scattering from the

stabilizer chains forming the micelle corona (as described by the Debye function within the scattering model, Equation *S7*) and also thermal fluctuations in the densities of the *n*-dodecane and/or copolymer components. Accordingly, constant background scattering has been incorporated into the model to account for this feature.

The two-population model produced a satisfactory fit to the nanoemulsion SAXS pattern (Figure 7). The lack of a well-defined minimum in the scattering curve suggests that the aqueous droplets are polydisperse in size, which is consistent with DLS and analytical centrifugation studies (see Table 1, entry e and Table 2, entry 3, respectively). A mean droplet diameter, D_{SAXS}, of 278 ± 68 nm was calculated using the two-population model from the core droplet diameter ($2R_c$) and mean shell thickness (T_{shell}) (Figure 7a). Bearing in mind the limited resolution at low *q,* this droplet diameter is in reasonably good agreement with DLS and analytical centrifugation data (272 ± 119 nm and 341 ± 326 nm, respectively). The mean apparent thickness of the adsorbed layer of nanoparticles, T_{shell}, obtained for this Pickering nanoemulsion was approximately 10 nm. Given that the $PSMA_{32}$ chains in direct contact with the surface of the aqueous droplets are most likely in their collapsed state, we estimate the effective thickness of an individual adsorbed nanoparticle to be 16.4 nm ($2R_s + 2R_g$) (see Figure 7b. Moreover, the micelle interaction radius obtained from SAXS analysis (R_{PY} = 20.7 nm) suggests that the nanoparticles are not in particularly close proximity to their neighbours, which results in an effective adsorbed layer thickness (T_{shell}) that is somewhat lower than the nanoparticle diameter. Thus, the SAXS data are consistent with the formation of a loosely packed monolayer of adsorbed nanoparticles surrounding each aqueous droplet, as expected for such a Pickering nanoemulsion.

It is well-known that o/w nanoemulsions undergo droplet growth predominantly via Ostwald ripening.[35-37] This phenomenon has also been reported for surfactant-stabilized w/o nanoemulsions.[16] To investigate the effect of varying the initial salt concentration on the rate

of Ostwald ripening, Pickering nanoemulsions were prepared using zero, 0.11 M or 0.44 M NaCl dissolved in the aqueous phase. DLS was used to monitor the number-average droplet radius (R_n) for the aged nanoemulsions. According to Lifshitz, Slyozov[101] and Wagner[102] (LSW theory), if the droplet growth mechanism occurs via Ostwald ripening then a plot of R_n^3 against time should be linear. This plot is shown in Figure 8a for a w/o Pickering nanoemulsion prepared in the absence of any added salt. Two distinct linear regimes are observed, with the rate of droplet growth increasing by an order of magnitude within 2 h. In contrast, R_n^3 increased linearly over time when the same w/o nanoemulsion was prepared using either 0.11 M or 0.43 M NaCl, indicating that droplet growth occurs via Ostwald ripening under such conditions (see Figure 8b).

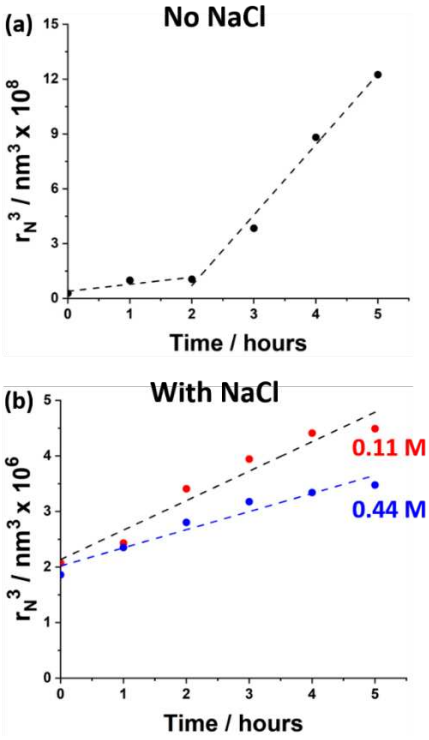

Figure 8. Variation in the cube of the mean droplet number-average radius (R_n) as determined by DLS over time at 20 °C for aged water-in-*n*-dodecane Pickering nanoemulsions prepared either (a) in the absence of NaCl or (b) using 0.11 M or 0.43 M NaCl dissolved in the aqueous phase prior to emulsification. In the absence of any salt, the growth of R_n^3 exhibits strongly non-linear behavior, with a clear breakpoint being observed after 2 h. However, a relatively linear relationship is observed in the presence of salt, suggesting that droplet growth under such conditions involves Ostwald ripening.

In each case, the fresh Pickering w/o nanoemulsion had an initial droplet diameter of approximately 250 nm. This is important when comparing such data, because the initial droplet

diameter (and polydispersity) is known to affect the rate of Ostwald ripening.[15] From the gradients of these linear plots, the Ostwald ripening rates were calculated to be 147 and 91 nm^3 s^{-1} for 0.11 M and 0.43 M NaCl, respectively. Thus, using a higher salt concentration leads to a slower rate of Ostwald ripening, as expected. This is because the salt ions are completely insoluble in the *n*-dodecane continuous phase and therefore remain within the aqueous droplets. Thus, if water molecules were to diffuse from small to large droplets, the salt concentration in the former droplets must increase, which would inevitably lead to a higher chemical potential. This retards the rate of mass transport of water from small to large aqueous droplets and explains why the addition of salt reduces the rate of Ostwald ripening of the aqueous droplets.[44-46]

Increasing the amount of added NaCl in the aqueous phase prior to high-shear homogenization leads to the formation of finer droplets and narrower size distributions. However, a limiting overall droplet diameter of around 250 nm is obtained at a critical concentration of 0.43 M NaCl. Thus, the effect of varying the NaCl concentration can be examined for w/o Pickering nanoemulsions with essentially the same initial mean droplet diameter. Analytical centrifugation was used to characterize both fresh and ageing nanoemulsions prepared using various salt concentrations. As noted by Thompson and co-workers, analytical centrifugation has a much higher resolution compared to DLS because droplet fractionation occurs prior to detection.[36] However, undersizing can be observed if the droplet concentration is too high owing to the phenomenon of hindered creaming.[36, 103] Moreover, using droplet concentrations that are too low can also be problematic: dilute emulsions scatter light only rather weakly and hence can fall outside of the optimum range required for the LUMiSizer instrument (i.e. below 30 % transmission). Given these conflicting requirements, Thompson and co-workers found that a droplet concentration of 1.0% v/v was optimal.[36] In the present study, the aqueous droplet concentration (or water volume fraction) used for analytical centrifugation studies was

systemically reduced. As shown in Figure S6, this led to a reduction in the apparent nanoemulsion droplet diameter, with a plateau value being observed at approximately 1.0% v/v. Analyzing more concentrated nanoemulsions leads to a significantly smaller apparent droplet diameter owing to hindered sedimentation. Therefore, each nanoemulsion was diluted to an aqueous droplet concentration of 1.0% v/v prior to analytical centrifugation experiments.

Table 2. Variation in Mean Droplet Diameter with Ageing Time as Determined by Analytical Centrifugation Analysis of Pickering Nanoemulsions Prepared Using 5.0% w/w $PSMA_9$-$PTFEMA_{50}$ Diblock Copolymer Nanoparticles with 0.05 M to 0.43 M NaCl Dissolved in the Aqueous Phase.

NaCl concentration / M	Volume-average droplet diameter by analytical centrifugation / nm				
	Fresh	1 week	2 weeks	3 weeks	4 weeks
0.43	259 ± 154	283 ± 220	276 ± 610	225 ± 227	229 ± 555
0.21	261 ± 178	297 ± 282	325 ± 872	342 ± 370	247 ± 566
0.11	341 ± 326	346 ± 1120	351 ± 1036	301 ± 537	257 ± 1128
0.05	463 ± 2522	918 ± 2395	828 ± 4225	522 ± 2901	498 ± 2103

Table 2 shows the mean volume-average diameters determined by analytical centrifugation for a series of w/o Pickering nanoemulsions prepared using 0.05 M to 0.43 M NaCl after ageing for up to 4 weeks at 20 °C. Unimodal droplet size distributions were observed for three of the four fresh nanoemulsions. The exception was the nanoemulsion prepared using 0.05 M NaCl, which exhibited a bimodal droplet size distribution. However, analysis of the latter fresh nanoemulsion by DLS indicated a unimodal droplet size distribution. In principle, this apparent discrepancy may simply reflect the inherently lower resolution of DLS compared to analytical centrifugation. Alternatively, Ostwald ripening may commence immediately after preparation of this relatively unstable nanoemulsion, with DLS merely offering a shorter analysis time. Nevertheless, aqueous droplets prepared using 0.05 M NaCl coarsened significantly faster relative to nanoemulsions prepared at higher salt concentrations. In all cases, both the volume-average droplet diameter and the corresponding polydispersity increased over a three-week period. However, a lower volume-average droplet diameter was observed after four weeks,

along with a concomitant increase in polydispersity. An apparent reduction in volume-average diameter was also reported by Thompson et al. during long-term ageing studies of o/w Pickering nanoemulsions stabilized by diblock copolymer nanoparticles, which was attributed to the increasingly skewed nature of the droplet size distribution.[36]

Figure 9a shows the volume-average cumulative distributions recorded for each of the four Pickering nanoemulsions after aging for 2 weeks at 20 °C. The greatest extent of Ostwald ripening is observed for the nanoemulsion prepared using 0.05 M NaCl, with more than 40% of the aqueous droplets now exceeding 2 μm diameter. In contrast, fewer than 5% of aqueous droplets exceed 2 μm after the same ageing time if they contain 0.11 M NaCl. Interestingly, no significant improvement in droplet stability is observed when using higher salt concentrations. After ageing for 2 weeks at 20 °C, most nanoemulsions exhibit bimodal droplet size distributions (see Figure 9b). Nanoemulsions prepared using 0.11 M NaCl or higher contain a minor population of larger droplets exceeding 2 μm diameter. For the least stable nanoemulsion prepared in the presence of 0.05 M NaCl, two approximately equal droplet populations are initially observed (see Figure 9a).

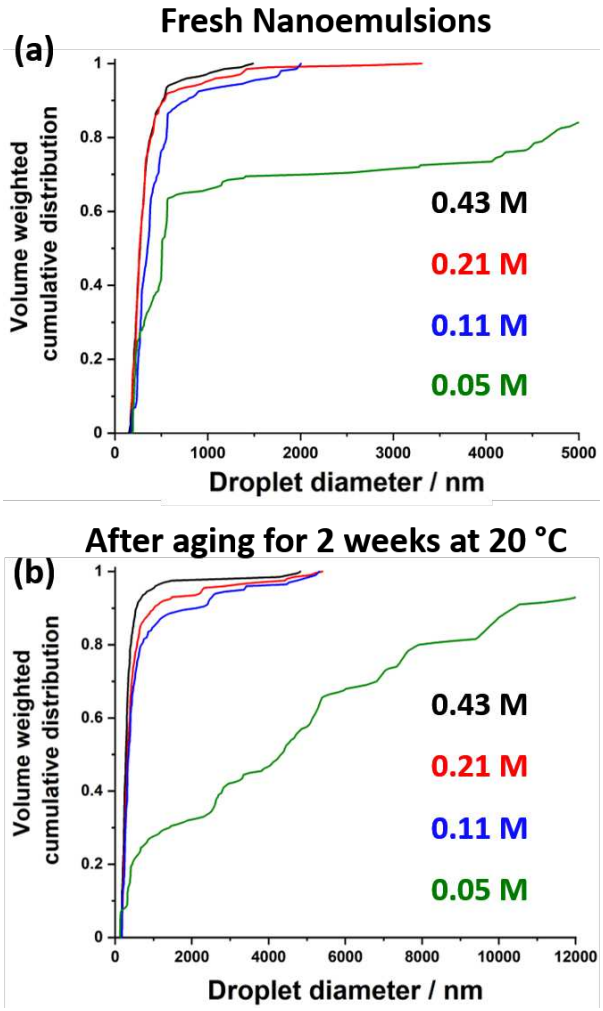

Figure 9. Volume-weighted cumulative distributions determined by analytical centrifugation (LUMiSizer instrument) for *n*-dodecane-in-water Pickering nanoemulsions prepared using various amounts of NaCl dissolved in the aqueous phase: (a) fresh nanoemulsions and (b) after aging for 2 weeks at 20 °C.

After ageing, the population of larger droplets has increased relative to that of the smaller droplets. Such observations are consistent with an Ostwald ripening mechanism and also account for the apparent reduction in droplet diameter that is observed after 4 weeks ageing at 20 °C (see Figure S7).

CONCLUSIONS

RAFT dispersion polymerization of TFEMA enables the convenient synthesis of sterically-stabilized $PSMA_{32}$–$PTFEMA_{53}$ spherical nanoparticles of 28 ± 6 nm diameter in *n*-dodecane at 80 °C. Such diblock copolymer nanoparticles have been used as an emulsifier to prepare the first example of a water-in-oil Pickering nanoemulsion. In the absence of any added salt in the dispersed aqueous phase, only relatively coarse droplets of more than 600 nm diameter could be produced via high-pressure microfluidization. However, increasing the NaCl concentration in the aqueous phase prior to emulsification led to a systematic reduction in the intensity-average droplet diameter, as judged by DLS studies. A limiting aqueous droplet diameter of around 250 nm was obtained when using 0.11 M NaCl. Furthermore, this droplet diameter could be tuned by varying the applied pressure and the number of passes through the microfluidizer. Increasing the $PSMA_{32}$-$PTFEMA_{53}$ nanoparticle concentration produced smaller water droplets, suggesting that such nanoparticles survive the microfluidization conditions intact. Furthermore, TEM studies conducted on the dried droplets confirm that the $PSMA_{32}$-$PTFEMA_{53}$ nanoparticles retain their original spherical morphology and adsorb intact at oil-water interface. SAXS studies conducted on such Pickering nanoemulsions confirm the formation of a loosely-packed monolayer of adsorbed nanoparticles surrounding the aqueous droplets. DLS studies indicate that the long-term stability of the aqueous droplets is enhanced at higher NaCl concentrations. The cube of the droplet radius of Pickering nanoemulsions prepared using an aqueous solution containing either 0.11 or 0.43 M NaCl increased linearly over time, suggesting that droplet growth involves an Ostwald ripening mechanism. In contrast, when such Pickering nanoemulsion were prepared in the absence of NaCl, they proved to be significantly less stable. Longer-term stability studies were also conducted on such nanoemulsions using analytical centrifugation. Ostwald ripening was substantially suppressed in the presence of 0.05 M NaCl, with volume-average diameters remaining below 300 nm after

4 weeks storage at 20 °C. However, using 0.11 M NaCl led to no discernible improvement in the nanoemulsion stability.

ASSOCIATED CONTENT

Supporting Information

^{19}F NMR spectrum recorded for $PSMA_{32}$-$PTFEMA_{53}$ diblock copolymer; DLS droplet diameter vs. applied pressure plot for Pickering nanoemulsions prepared in the absence of any NaCl; z-average droplet distributions determined by DLS for Pickering nanoemulsions prepared at either pH 2 or pH 7; digital photographs recorded for one-day old Pickering nanoemulsions prepared using up to 0.11 M NaCl; effect of varying the water volume fraction on the volume-average droplet diameter as determined by analytical centrifugation; Volume-weighted cumulative distributions recorded for Pickering nanoemulsions prepared using 0.05-0.43 M NaCl after ageing for 4 weeks at 20 °C; scattering models used for SAXS analysis.

This material is available free of charge via the Internet at http//:pubs.acs.org

AUTHOR INFORMATION

Corresponding Authors

*Email s.p.armes@shef.ac.uk (S.P.A.)

The manuscript was written through contributions of all authors. All authors have given approval to the final version of the manuscript.

Funding Sources: EPSRC and DSM (Geleen, The Netherlands).

ACKNOWLEDGMENTS

EPSRC is thanked for a CDT PhD studentship to support S.J.H. (EP/L016281) and also an Established Career Particle Technology Fellowship (EP/R003009) for S.P.A. O.O.M and S.P.A. also thanks EPSRC for the capital equipment grant (EP/M028437/1) to purchase the laboratory-based Xenocs Xeuss 2.0/Excillum SAXS beamline used for the SAXS data collection. DSM (Geleen, The Netherlands) is acknowledged for partial support of this PhD project and for permission to publish this work. The authors thank Christopher Hill and Dr. Svetomir Tzokov at the University of Sheffield Biomedical Science Electron Microscopy suite.

REFERENCES

1. Pickering, S. U., Emulsions. *J. Chem. Soc.* **1907,** *91*, 2001-2021.

2. Ramsden, W., Separation of Solids in the Surface-Layers of Solutions and 'Suspensions' (Observations on Surface-Membranes, Bubbles, Emulsions, and Mechanical Coagulation). -- Preliminary Account. *Proc. R. Soc. London* **1903,** *72*, 156-164.

3. Binks, B. P., Particles as surfactants—similarities and differences. *Curr. Opin. Colloid Interface Sci.* **2002,** *7*, 21-41.

4. Wilde, P., Interfaces: Their role in foam and emulsion behaviour. *Current Opinion in Colloid & Interface Science - CURR OPIN COLLOID INTERFACE S* **2000,** *5*, 176-181.

5. Kabalnov, A., Thermodynamic and theoretical aspects of emulsions and their stability. *Curr. Opin. Colloid Interface Sci.* **1998,** *3*, 270-275.

6. Hsu, J.-P.; Nacu, A., Behavior of soybean oil-in-water emulsion stabilized by nonionic surfactant. *J. Colloid Interface Sci.* **2003,** *259*, 374-381.

7. Opawale, F. O.; Burgess, D. J., Influence of Interfacial Properties of Lipophilic Surfactants on Water-in-Oil Emulsion Stability. *J. Colloid Interface Sci.* **1998,** *197*, 142-150.

8. Binks, B. P.; Lumsdon, S. O., Influence of Particle Wettability on the Type and Stability of Surfactant-Free Emulsions. *Langmuir* **2000,** *16*, 8622-8631.

9. P. Binks, B.; O. Lumsdon, S., Stability of oil-in-water emulsions stabilised by silica particles. *Phys. Chem. Chem. Phys.* **1999,** *1*, 3007-3016.

10. Binks, B. P.; Lumsdon, S. O., Catastrophic Phase Inversion of Water-in-Oil Emulsions Stabilized by Hydrophobic Silica. *Langmuir* **2000,** *16*, 2539-2547.

11. Binks, B. P.; Lumsdon, S. O., Pickering Emulsions Stabilized by Monodisperse Latex Particles: Effects of Particle Size. *Langmuir* **2001,** *17*, 4540-4547.

12. Binks, B. P.; Whitby, C. P., Nanoparticle silica-stabilised oil-in-water emulsions: improving emulsion stability. *Colloids Surf., A* **2005,** *253*, 105-115.

13. Solans, C.; Izquierdo, P.; Nolla, J.; Azemar, N.; Garcia-Celma, M. J., Nano-emulsions. *Curr. Opin. Colloid Interface Sci.* **2005,** *10*, 102-110.

14. McClements, D. J., Nanoemulsions versus microemulsions: terminology, differences, and similarities. *Soft Matter* **2012,** *8*, 1719-1729.

15. Gupta, A.; Eral, H. B.; Hatton, T. A.; Doyle, P. S., Nanoemulsions: formation, properties and applications. *Soft Matter* **2016,** *12*, 2826-2841.

16. Sommerling, J.-H.; de Matos, M. B. C.; Hildebrandt, E.; Dessy, A.; Kok, R. J.; Nirschl, H.; Leneweit, G., Instability Mechanisms of Water-in-Oil Nanoemulsions with Phospholipids: Temporal and Morphological Structures. *Langmuir* **2018,** *34*, 572-584.

17. Massel, V.; Alexander, M.; Corredig, M., The Colloidal Behavior of Pectin Containing Water in Oil Emulsions as a Function of Emulsifier Concentration. *Food Biophysics* **2015,** *10*, 57-65.

18. Zhu, Q.; Wu, F.; Saito, M.; Tatsumi, E.; Yin, L., Effect of magnesium salt concentration in water-in-oil emulsions on the physical properties and microstructure of tofu. *Food Chemistry* **2016,** *201*, 197-204.

19. Peng, L. C.; Liu, C. H.; Kwan, C. C.; Huang, K. F., Optimization of water-in-oil nanoemulsions by mixed surfactants. *Colloids and Surfaces a-Physicochemical and Engineering Aspects* **2010,** *370*, 136-142.

20. Machado, A. H. E.; Lundberg, D.; Ribeiro, A. J.; Veiga, F. J.; Lindman, B.; Miguel, M. G.; Olsson, U., Preparation of Calcium Alginate Nanoparticles Using Water-in-Oil (W/O) Nanoemulsions. *Langmuir* **2012,** *28*, 4131-4141.

21. Chiesa, M.; Garg, J.; Kang, Y. T.; Chen, G., Thermal conductivity and viscosity of water-in-oil nanoemulsions. *Colloids Surf., A* **2008,** *326*, 67-72.

22. Lee, L.; Hancocks, R.; Noble, I.; Norton, I. T., Production of water-in-oil nanoemulsions using high pressure homogenisation: A study on droplet break-up. *J. Food Eng.* **2014,** *131*, 33-37.

23. Orte, A.; Ruedas-Rama, M. J.; Paredes, J. M.; Crovetto, L.; Alvarez-Pez, J. M., Dynamics of Water-in-Oil Nanoemulsions Revealed by Fluorescence Lifetime Correlation Spectroscopy. *Langmuir* **2011,** *27*, 12792-12799.

24. Kumar, H.; Kumar, V., Ultrasonication assisted formation and stability of water-in-oil nanoemulsions: Optimization and ternary diagram analysis. *Ultrason. Sonochem.* **2018,** *49*, 79-88.

25. Guha, I. F.; Anand, S.; Varanasi, K. K., Creating nanoscale emulsions using condensation. *Nat. Commun.* **2017,** *8*, 7.

26. Kini, G. C.; Biswal, S. L.; Wong, M. S.; Miller, C. A., Characteristics of spontaneously formed nanoemulsions in octane/AOT/brine systems. *J. Colloid Interface Sci.* **2012,** *385*, 111-121.

27. Anton, N.; Saulnier, P., Adhesive water-in-oil nano-emulsions generated by the phase inversion temperature method. *Soft Matter* **2013,** *9*, 6465-6474.

28. Wu, H.; Ramachandran, C.; Weiner, N. D.; Roessler, B. J., Topical transport of hydrophilic compounds using water-in-oil nanoemulsions. *Int J Pharm* **2001,** *220*, 63-75.

29. Wu, H.; Ramachandran, C.; Bielinska, A. U.; Kingzett, K.; Sun, R.; Weiner, N. D.; Roessler, B. J., Topical transfection using plasmid DNA in a water-in-oil nanoemulsion. *Int J Pharm* **2001,** *221*, 23-34.

30. Shakeel, F.; Ramadan, W., Transdermal delivery of anticancer drug caffeine from water-in-oil nanoemulsions. *Colloids and Surfaces B: Biointerfaces* **2010,** *75*, 356-362.

31. Wang, J. J.; Hung, C. F.; Yeh, C. H.; Fang, J. Y., The release and analgesic activities of morphine and its ester prodrug, morphine propionate, formulated by water-in-oil nanoemulsions. *J. Drug Target.* **2008,** *16*, 294-301.

32. McClements, D. J.; Rao, J., Food-Grade Nanoemulsions: Formulation, Fabrication, Properties, Performance, Biological Fate, and Potential Toxicity. *Critical Reviews in Food Science and Nutrition* **2011,** *51*, 285-330.

33. McClements, D. J., Edible nanoemulsions: fabrication, properties, and functional performance. *Soft Matter* **2011,** *7*, 2297-2316.

34. Sonneville-Aubrun, O.; Simonnet, J. T.; L'Alloret, F., Nanoemulsions: a new vehicle for skincare products. *Adv. Colloid Interface Sci.* **2004,** *108-109*, 145-149.

35. Persson, K. H.; Blute, I. A.; Mira, I. C.; Gustafsson, J., Creation of well-defined particle stabilized oil-in-water nanoemulsions. *Colloids Surf., A* **2014,** *459*, 48-57.

36. Thompson, K. L.; Derry, M. J.; Hatton, F. L.; Armes, S. P., Long-Term Stability of n-Alkane-in-Water Pickering Nanoemulsions: Effect of Aqueous Solubility of Droplet Phase on Ostwald Ripening. *Langmuir* **2018,** *34*, 9289-9297.

37. Rodriguez-Lopez, G.; O'Neil Williams, Y.; Toro-Mendoza, J., Individual and Collective Behavior of Emulsion Droplets Undergoing Ostwald Ripening. *Langmuir* **2019,** *35*, 5316-5323.

38. Kabal'nov, A. S.; Pertzov, A. V.; Shchukin, E. D., Ostwald ripening in two-component disperse phase systems: Application to emulsion stability. *Colloids Surf.* **1987,** *24*, 19-32.

39. Webster, A. J.; Cates, M. E., Stabilization of Emulsions by Trapped Species. *Langmuir* **1998,** *14*, 2068-2079.

40. Kabalnov, A., Ostwald Ripening and Related Phenomena. *Journal of Dispersion Science and Technology* **2001,** *22*, 1-12.

41. Egger, H.; McGrath, K. M., Aging of oil-in-water emulsions: The role of the oil. *J. Colloid Interface Sci.* **2006,** *299*, 890-899.

42. Wooster, T. J.; Golding, M.; Sanguansri, P., Impact of Oil Type on Nanoemulsion Formation and Ostwald Ripening Stability. *Langmuir* **2008,** *24*, 12758-12765.

43. Delmas, T.; Piraux, H.; Couffin, A.-C.; Texier, I.; Vinet, F.; Poulin, P.; Cates, M. E.; Bibette, J., How To Prepare and Stabilize Very Small Nanoemulsions. *Langmuir* **2011,** *27*, 1683-1692.

44. Kizling, J.; Kronberg, B., On the formation and stability of concentrated water-in-oil emuslions, aphrons. *Colloids Surf.* **1990,** *50*, 131-140.

45. Koroleva, M. Y.; Yurtov, E. V., Effect of ionic strength of dispersed phase on Ostwald ripening in water-in-oil emulsions. *Colloid Journal* **2003,** *65*, 40-43.

46. Aronson, M. P.; Petko, M. F., Highly Concentrated Water-in-Oil Emulsions: Influence of Electrolyte on Their Properties and Stability. *J. Colloid Interface Sci.* **1993,** *159*, 134-149.

47. Eskandar, N. G.; Simovic, S.; Prestidge, C. A., Interactions of hydrophilic silica nanoparticles and classical surfactants at non-polar oil–water interface. *J. Colloid Interface Sci.* **2011,** *358*, 217-225.

48. Thompson, K. L.; Cinotti, N.; Jones, E. R.; Mable, C. J.; Fowler, P. W.; Armes, S. P., Bespoke Diblock Copolymer Nanoparticles Enable the Production of Relatively Stable Oil-in-Water Pickering Nanoemulsions. *Langmuir* **2017,** *33*, 12616-12623.

49. Jiménez Saelices, C.; Capron, I., Design of Pickering Micro- and Nanoemulsions Based on the Structural Characteristics of Nanocelluloses. *Biomacromolecules* **2018,** *19*, 460-469.

50. Kang, D. J.; Bararnia, H.; Anand, S., Synthesizing Pickering Nanoemulsions by Vapor Condensation. *ACS Applied Materials & Interfaces* **2018,** *10*, 21746-21754.

51. Du, Z.; Li, Q.; Li, J.; Su, E.; Liu, X.; Wan, Z.; Yang, X., Self-Assembled Egg Yolk Peptide Micellar Nanoparticles as a Versatile Emulsifier for Food-Grade Oil-in-Water Pickering Nanoemulsions. *J Agr Food Chem* **2019,** *67*, 11728-11740.

52. Dieng, S. M.; Anton, N.; Bouriat, P.; Thioune, O.; Sy, P. M.; Massaddeq, N.; Enharrar, S.; Diarra, M.; Vandamme, T., Pickering nano-emulsions stabilized by solid lipid nanoparticles as a temperature sensitive drug delivery system. *Soft Matter* **2019**.

53. Hunter, S. J.; Penfold, N. J. W.; Chan, D. H.; Mykhaylyk, O. O.; Armes, S. P., How Do Charged End-Groups on the Steric Stabilizer Block Influence the Formation and Long-Term Stability of Pickering Nanoemulsions Prepared Using Sterically Stabilized Diblock Copolymer Nanoparticles? *Langmuir* **2020,** *36*, 769-780.

54. Xiao, Z.; Liu, Y.; Niu, Y.; Kou, X., Cyclodextrin supermolecules as excellent stabilizers for Pickering nanoemulsions. *Colloids Surf., A* **2020,** *588*, 124367.

55. Jiang, H.; Hong, L.; Li, Y.; Ngai, T., All-Silica Submicrometer Colloidosomes for Cargo Protection and Tunable Release. *Angew. Chem. Int. Ed.* **2018,** *57*, 11662-11666.

56. Sihler, S.; Schrade, A.; Cao, Z.; Ziener, U., Inverse Pickering Emulsions with Droplet Sizes below 500 nm. *Langmuir* **2015,** *31*, 10392-10401.

57. Bollhorst, T.; Grieb, T.; Rosenauer, A.; Fuller, G.; Maas, M.; Rezwan, K., Synthesis Route for the Self-Assembly of Submicrometer-Sized Colloidosomes with Tailorable Nanopores. *Chemistry of Materials* **2013,** *25*, 3464-3471.

58. Canning, S. L.; Smith, G. N.; Armes, S. P., A Critical Appraisal of RAFT-Mediated Polymerization-Induced Self-Assembly. *Macromolecules* **2016,** *49*, 1985-2001.

59. Cunningham, V. J.; Alswieleh, A. M.; Thompson, K. L.; Williams, M.; Leggett, G. J.; Armes, S. P.; Musa, O. M., Poly(glycerol monomethacrylate)–Poly(benzyl methacrylate) Diblock Copolymer Nanoparticles via RAFT Emulsion Polymerization: Synthesis, Characterization, and Interfacial Activity. *Macromolecules* **2014,** *47*, 5613-5623.

60. Jones, E. R.; Semsarilar, M.; Blanazs, A.; Armes, S. P., Efficient Synthesis of Amine-Functional Diblock Copolymer Nanoparticles via RAFT Dispersion Polymerization of Benzyl Methacrylate in Alcoholic Media. *Macromolecules* **2012,** *45*, 5091-5098.

61. Warren, N. J.; Armes, S. P., Polymerization-Induced Self-Assembly of Block Copolymer Nano-objects via RAFT Aqueous Dispersion Polymerization. *J. Am. Chem. Soc.* **2014,** *136*, 10174-10185.

62. Akpinar, B.; Fielding, L. A.; Cunningham, V. J.; Ning, Y.; Mykhaylyk, O. O.; Fowler, P. W.; Armes, S. P., Determining the Effective Density and Stabilizer Layer Thickness of Sterically Stabilized Nanoparticles. *Macromolecules* **2016,** *49*, 5160-5171.

63. Hatton, F. L.; Lovett, J. R.; Armes, S. P., Synthesis of well-defined epoxy-functional spherical nanoparticles by RAFT aqueous emulsion polymerization. *Polym. Chem.* **2017,** *8*, 4856-4868.

64. Mable, C. J.; Warren, N. J.; Thompson, K. L.; Mykhaylyk, O. O.; Armes, S. P., Framboidal ABC triblock copolymer vesicles: a new class of efficient Pickering emulsifier. *Chem. Sci.* **2015,** *6*, 6179-6188.

65. Blanazs, A.; Madsen, J.; Battaglia, G.; Ryan, A. J.; Armes, S. P., Mechanistic Insights for Block Copolymer Morphologies: How Do Worms Form Vesicles? *J. Am. Chem. Soc.* **2011,** *133*, 16581-16587.

66. Ratcliffe, L. P. D.; Blanazs, A.; Williams, C. N.; Brown, S. L.; Armes, S. P., RAFT polymerization of hydroxy-functional methacrylic monomers under heterogeneous conditions: effect of varying the core-forming block. *Polym. Chem.* **2014,** *5*, 3643-3655.

67. Jiang, Y.; Xu, N.; Han, J.; Yu, Q.; Guo, L.; Gao, P.; Lu, X.; Cai, Y., The direct synthesis of interface-decorated reactive block copolymer nanoparticles via polymerisation-induced self-assembly. *Polym. Chem.* **2015,** *6*, 4955-4965.

68. Shen, W.; Chang, Y.; Liu, G.; Wang, H.; Cao, A.; An, Z., Biocompatible, Antifouling, and Thermosensitive Core−Shell Nanogels Synthesized by RAFT Aqueous Dispersion Polymerization. *Macromolecules* **2011,** *44*, 2524-2530.

69. Pei, Y.; Dharsana, N. C.; van Hensbergen, J. A.; Burford, R. P.; Roth, P. J.; Lowe, A. B., RAFT dispersion polymerization of 3-phenylpropyl methacrylate with poly[2-(dimethylamino)ethyl methacrylate] macro-CTAs in ethanol and associated thermoreversible polymorphism. *Soft Matter* **2014,** *10*, 5787-5796.

70. Pei, Y.; Lowe, A. B., Polymerization-induced self-assembly: ethanolic RAFT dispersion polymerization of 2-phenylethyl methacrylate. *Polym. Chem.* **2014,** *5*, 2342-2351.

71. Pei, Y.; Dharsana, N. C.; Lowe, A. B., Ethanolic RAFT Dispersion Polymerization of 2-(Naphthalen-2-yloxy)ethyl Methacrylate and 2-Phenoxyethyl Methacrylate with Poly[2-(dimethylamino)ethyl Methacrylate] Macro-Chain Transfer Agents. *Aust. J. Chem.* **2015,** *68*, 939-945.

72. Pei, Y.; Jarrett, K.; Saunders, M.; Roth, P. J.; Buckley, C. E.; Lowe, A. B., Triply responsive soft matter nanoparticles based on poly[oligo(ethylene glycol) methyl ether methacrylate-block-3-phenylpropyl methacrylate] copolymers. *Polym. Chem.* **2016,** *7*, 2740-2750.

73. Semsarilar, M.; Jones, E. R.; Blanazs, A.; Armes, S. P., Efficient Synthesis of Sterically-Stabilized Nano-Objects via RAFT Dispersion Polymerization of Benzyl Methacrylate in Alcoholic Media. *Adv. Mater.* **2012,** *24*, 3378-3382.

74. Gonzato, C.; Semsarilar, M.; Jones, E. R.; Li, F.; Krooshof, G. J. P.; Wyman, P.; Mykhaylyk, O. O.; Tuinier, R.; Armes, S. P., Rational Synthesis of Low-Polydispersity Block Copolymer Vesicles in Concentrated Solution via Polymerization-Induced Self-Assembly. *J. Am. Chem. Soc.* **2014,** *136*, 11100-11106.

75. Yang, P.; Mykhaylyk, O. O.; Jones, E. R.; Armes, S. P., RAFT Dispersion Alternating Copolymerization of Styrene with N-Phenylmaleimide: Morphology Control and Application as an Aqueous Foam Stabilizer. *Macromolecules* **2016,** *49*, 6731-6742.

76. Semsarilar, M.; Penfold, N. J. W.; Jones, E. R.; Armes, S. P., Semi-crystalline diblock copolymer nano-objects prepared via RAFT alcoholic dispersion polymerization of stearyl methacrylate. *Polym. Chem.* **2015,** *6*, 1751-1757.

77. Jones, E. R.; Semsarilar, M.; Wyman, P.; Boerakker, M.; Armes, S. P., Addition of water to an alcoholic RAFT PISA formulation leads to faster kinetics but limits the evolution of copolymer morphology. *Polym. Chem.* **2016,** *7*, 851-859.

78. Houillot, L.; Bui, C.; Save, M.; Charleux, B.; Farcet, C.; Moire, C.; Raust, J.-A.; Rodriguez, I., Synthesis of Well-Defined Polyacrylate Particle Dispersions in Organic Medium Using Simultaneous RAFT Polymerization and Self-Assembly of Block Copolymers. A Strong Influence of the Selected Thiocarbonylthio Chain Transfer Agent. *Macromolecules* **2007,** *40*, 6500-6509.

79. Fielding, L. A.; Derry, M. J.; Ladmiral, V.; Rosselgong, J.; Rodrigues, A. M.; Ratcliffe, L. P. D.; Sugihara, S.; Armes, S. P., RAFT dispersion polymerization in non-polar solvents: facile production of block copolymer spheres, worms and vesicles in n-alkanes. *Chem. Sci.* **2013,** *4*, 2081-2087.

80. Derry, M. J.; Fielding, L. A.; Armes, S. P., Polymerization-induced self-assembly of block copolymer nanoparticles via RAFT non-aqueous dispersion polymerization. *Progress in Polymer Science* **2016,** *52*, 1-18.

81. Fielding, L. A.; Lane, J. A.; Derry, M. J.; Mykhaylyk, O. O.; Armes, S. P., Thermo-responsive Diblock Copolymer Worm Gels in Non-polar Solvents. *J. Am. Chem. Soc.* **2014,** *136*, 5790-5798.

82. Derry, M. J.; Fielding, L. A.; Armes, S. P., Industrially-relevant polymerization-induced self-assembly formulations in non-polar solvents: RAFT dispersion polymerization of benzyl methacrylate. *Polym. Chem.* **2015,** *6*, 3054-3062.

83. Pei, Y.; Sugita, O. R.; Thurairajah, L.; Lowe, A. B., Synthesis of poly(stearyl methacrylate-b-3-phenylpropyl methacrylate) nanoparticles in n-octane and associated thermoreversible polymorphism. *RSC Advances* **2015,** *5*, 17636-17646.

84. Pei, Y.; Thurairajah, L.; Sugita, O. R.; Lowe, A. B., RAFT Dispersion Polymerization in Nonpolar Media: Polymerization of 3-Phenylpropyl Methacrylate in n-Tetradecane with Poly(stearyl methacrylate) Homopolymers as Macro Chain Transfer Agents. *Macromolecules* **2015,** *48*, 236-244.

85. Ratcliffe, L. P. D.; McKenzie, B. E.; Le Bouëdec, G. M. D.; Williams, C. N.; Brown, S. L.; Armes, S. P., Polymerization-Induced Self-Assembly of All-Acrylic Diblock Copolymers via RAFT Dispersion Polymerization in Alkanes. *Macromolecules* **2015,** *48*, 8594-8607.

86. Rymaruk, M. J.; Hunter, S. J.; O'Brien, C. T.; Brown, S. L.; Williams, C. N.; Armes, S. P., RAFT Dispersion Polymerization in Silicone Oil. *Macromolecules* **2019,** *52*, 2822-2832.

87. György, C.; Hunter, S. J.; Girou, C.; Derry, M. J.; Armes, S. P., Synthesis of poly(stearyl methacrylate)-poly(2-hydroxypropyl methacrylate) diblock copolymer nanoparticles via RAFT dispersion polymerization of 2-hydroxypropyl methacrylate in mineral oil. *Polym. Chem.* **2020,** *11*, 4579-4590.

88. Thompson, K. L.; Chambon, P.; Verber, R.; Armes, S. P., Can Polymersomes Form Colloidosomes? *J. Am. Chem. Soc.* **2012,** *134*, 12450-12453.

89. Thompson, K. L.; Lane, J. A.; Derry, M. J.; Armes, S. P., Non-aqueous Isorefractive Pickering Emulsions. *Langmuir* **2015,** *31*, 4373-4376.

90. Rizzelli, S. L.; Jones, E. R.; Thompson, K. L.; Armes, S. P., Preparation of non-aqueous Pickering emulsions using anisotropic block copolymer nanoparticles. *Colloid. Polym. Sci.* **2016,** *294*, 1-12.

91. Thompson, K. L.; Fielding, L. A.; Mykhaylyk, O. O.; Lane, J. A.; Derry, M. J.; Armes, S. P., Vermicious thermo-responsive Pickering emulsifiers. *Chem. Sci.* **2015,** *6*, 4207-4214.

92. Thompson, K. L.; Mable, C. J.; Lane, J. A.; Derry, M. J.; Fielding, L. A.; Armes, S. P., Preparation of Pickering Double Emulsions Using Block Copolymer Worms. *Langmuir* **2015,** *31*, 4137-4144.

93. Semsarilar, M.; Ladmiral, V.; Blanazs, A.; Armes, S. P., Anionic Polyelectrolyte-Stabilized Nanoparticles via RAFT Aqueous Dispersion Polymerization. *Langmuir* **2012,** *28*, 914-922.

94. Cornel, E. J.; van Meurs, S.; Smith, T.; O'Hora, P. S.; Armes, S. P., In Situ Spectroscopic Studies of Highly Transparent Nanoparticle Dispersions Enable Assessment of Trithiocarbonate Chain-End Fidelity during RAFT Dispersion Polymerization in Nonpolar Media. *J. Am. Chem. Soc.* **2018,** *140*, 12980-12988.

95. Gates, J. A.; Wood, R. H., Densities of aqueous solutions of sodium chloride, magnesium chloride, potassium chloride, sodium bromide, lithium chloride, and calcium chloride from 0.05 to 5.0 mol kg-1 and 0.1013 to 40 MPa at 298.15 K. *Journal of Chemical & Engineering Data* **1985,** *30*, 44-49.

96. Ilavsky, J.; Jemian, P. R., Irena: tool suite for modeling and analysis of small-angle scattering. *J. Appl. Crystallogr.* **2009,** *42*, 347-353.

97. Balmer, J. A.; Armes, S. P.; Fowler, P. W.; Tarnai, T.; Gáspár, Z.; Murray, K. A.; Williams, N. S. J., Packing Efficiency of Small Silica Particles on Large Latex Particles: A Facile Route to Colloidal Nanocomposites. *Langmuir* **2009,** *25*, 5339-5347.

98. Pedersen, J. S.; Gerstenberg, M. C., Scattering Form Factor of Block Copolymer Micelles. *Macromolecules* **1996,** *29*, 1363-1365.

99. Pawlik, A.; Cox, P. W.; Norton, I. T., Food grade duplex emulsions designed and stabilised with different osmotic pressures. *J. Colloid Interface Sci.* **2010,** *352*, 59-67.

100. Kalashnikova, I.; Bizot, H.; Bertoncini, P.; Cathala, B.; Capron, I., Cellulosic nanorods of various aspect ratios for oil in water Pickering emulsions. *Soft Matter* **2013,** *9*, 952-959.

101. Lifshitz, I. M.; Slyozov, V. V., The kinetics of precipitation from supersaturated solid solutions. *Journal of Physics and Chemistry of Solids* **1961,** *19*, 35-50.

102. Wagner, C., Theorie der Alterung von Niederschlägen durch Umlösen (Ostwald-Reifung). *Zeitschrift für Elektrochemie, Berichte der Bunsengesellschaft für physikalische Chemie* **1961,** *65*, 581-591.

103. Walter, J.; Thajudeen, T.; Su, S.; Segets, D.; Peukert, W., New possibilities of accurate particle characterisation by applying direct boundary models to analytical centrifugation. *Nanoscale* **2015,** *7*, 6574-6587.